ISSN 1392-1207. MECHANIKA. Vol. 32, No. 5, 2026: 412–419

Thermo-Mechanical Coupling Simulation and Process Research of Gun Drilling for 15-15hs Max High-Nitrogen Non-Magnetic Steel with Ultra-Large Length-To-Diameter Ratio

Sang FENG*, Yanfei GONG*, Guanyun ZENG**
**School of Electromechanical Engineering, Guangdong University of Technology, Guangzhou Guangdong 510006, China, E-mail: fengsang@gdut.edu.cn (Corresponding Author: Sang FENG)*
***Huizhou Desay SV Automotive Electronics Co., Ltd., Huizhou Guangdong 516000, China, E-mail: 19864643259@163.com*
https://doi.org/10.5755/j02.mech.39661

1 Introduction

High-nitrogen austenitic stainless steel 15-15hs Max (UNS S20910 / Nitronic 50) achieves austenite stabilization and significant strengthening through solid-solution nitrogen of 0.5–0.8 wt.%, with a yield strength reaching 2-3 times that of conventional 304 stainless steel. It maintains extremely low magnetic permeability and excellent corrosion resistance in harsh environments containing H_2S/CO_2, making it a preferred material for key components in energy equipment, aerospace, and chemical industries [1-4]. However, its low thermal conductivity (approximately 13.8 $W \cdot m^{-1} \cdot K^{-1}$, only 2/3 of that of 304 stainless steel), high work hardening rate, and large cutting resistance cause heat to be difficult to dissipate quickly through convection and conduction in the semi-closed cutting conditions of deep hole gun drilling with a diameter of ∅5 mm and an ultra-large length-to-diameter ratio (L/D = 240), leading to cutting heat accumulation and accelerated tool wear or even tool breakage [5].

Gun drilling is the mainstream process for small-diameter (D < 20 mm) deep hole machining, in which cutting fluid is supplied through the inner hole of the drill rod and chips are expelled along the external V-shaped groove of the drill rod. The heat dissipation at the cutting edge primarily relies on high-pressure cooling fluid flushing rather than natural convection. In the CIRP Annals review of deep hole drilling, Biermann et al. [6] clearly pointed out that for difficult-to-machine materials, thermal management is the core bottleneck of deep hole process reliability, rather than simply pursuing the highest material removal rate. Yıldız et al. [7] used DEFORM-3D to simulate the drilling thrust and interface temperature of UNS S31603; Lotfi et al. [8] established a thermo-wear coupling model related to the Usui wear rate in drilling of AISI 1045; Zhu et al. [9] reviewed the experimental and numerical research progress on temperature measurement of rotating cutting tools. In addition, Lou et al. [11] studied the chip formation in gun drilling of 304 stainless steel deep holes, and Li et al. [12] conducted simulation and experimental studies on drilling of 304 stainless steel, providing a benchmark comparison for the process parameter range setting in this paper. However, none of the above works have addressed the thermal field boundary and parameter safety window for gun drilling of 15-15hs Max, especially lacking reproducible data for ultra-deep holes with a length-to-diameter ratio exceeding 200, considering its characteristic low-thermal-conductivity and high-strength coupling.

Based on the previous work of the research group on cutting force and chip morphology characterization of 15-15hs Max gun drilling [10], this paper focuses on the following questions: how do rotational speed and feed rate drive the temperature rise in the cutting zone during ∅5 mm deep hole gun drilling of this material? To what level does temperature and tool stress accumulation trigger brittle failure of YG8 tools? How can stable machining parameter boundaries be established accordingly? These questions are answered through DEFORM-3D local model simulation and full-scale five-workpiece verification experiments. Since the workpiece blanks are special equipment components with a unit value of approximately several hundred thousand RMB (tens of thousands of euros), the trial cutting cost is high; therefore, this study did not establish a classical Taylor tool life curve, but directly used whether the tool broke as the engineering criterion for tool reliability, providing an engineering reference for the process parameter selection of deep hole gun drilling of the difficult-to-machine material 15-15hs Max. Given the extremely high unit value of the workpieces, this study did not adopt classical Taylor tool life statistics, but instead used zero tool breakage and hole axis precision as the dual criteria for process feasibility, defining the parameter safety window from the perspective of reliability engineering.

2. 15-15hs Max Material and Tool Characteristics

2.1. Main parameters of workpiece material

Compared with conventional chromium-manganese stainless steels, 15-15hs Max has a lower carbon content (≤0.04%), which reduces the tendency for carbide precipitation at grain boundaries, thereby improving its resistance to intergranular stress corrosion cracking. At the same time, its nitrogen content is relatively high (approximately 0.5-0.8 wt.%), and nitrogen plays an important role in improving the material strength [4]. The main physical and mechanical properties of 15-15hs Max are shown in Table 1.

This material exhibits the following characteristics during deep hole machining [5]: 1. High cutting temperature: due to its high strength and large unit cutting work, combined with low thermal conductivity, heat is not easily dissipated through the workpiece. 2. High cutting force: due to its high strength and toughness, larger cutting forces are required, significantly higher than those of conventional

Table 1
Typical physical and mechanical properties of 15-15hs Max

Property	Value	Unit
Density	7.75	$g \cdot cm^{-3}$
Elastic modulus	191	GPa
Poisson ratio	0.3	—
Yield strength	≥1118	MPa
Thermal conductivity (20 °C)	≈13.8	$W \cdot m^{-1} \cdot K^{-1}$
Thermal expansion coefficient	19.3	$10^{-6} \cdot K^{-1}$

structural steels. 3. Severe work hardening: plastic deformation during machining leads to significant work hardening. The research of Pang et al. [5] showed that for turning and other open cutting conditions, work hardening of high-nitrogen austenitic stainless steel decreases markedly and stabilizes when the cutting speed exceeds approximately 80 m/min. However, due to the hole diameter restriction in deep hole gun drilling, the maximum cutting speed in this paper is only about 22 m/min, far below this threshold, so the work hardening effect remains significant throughout the entire parameter range. 4. Rapid tool wear: the enclosed machining environment restricts direct flushing of the cutting edge by cooling fluid, leading to severe tool wear.

2.2. Tool material characteristics

A gun drill mainly consists of a drill bit, drill rod, and drill handle, with each component connected through welding. The drill bit typically employs high-hardness alloys, mostly tungsten-cobalt cemented carbides such as YG6 and YG8 [6, 13]. The structure of the gun drill is shown in Fig. 1. The geometric parameters of the gun drill are set according to the gun drill tip modeling standard [13].

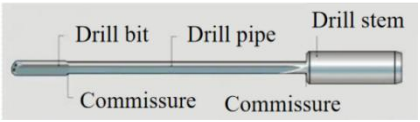

Fig.1 Structure diagram of gun drill

YG8 cemented carbide (WC-8%Co) is commonly used as a tool material for drilling difficult-to-machine materials due to its high strength, good impact resistance and vibration damping performance, high bending strength (≥1800 MPa), and thermal conductivity [14]. The main performance parameters of YG8 are shown in Table 2.

In the first full-scale trial cutting experiment, an uncoated YG8 tool was used, and fracture occurred at approximately 670 mm. In the subsequent verification experiment, an AlTi-coated YG8-based gun drill was adopted to improve the wear resistance and thermal softening resistance of the cutting edge. It should be noted that the simulation model in this paper was established based on uncoated YG8, with a friction coefficient of 0.75, and the temperature field results correspond to the uncoated condition. The AlTi coating reduces the tool-chip friction coefficient and produces a thermal barrier effect, so the actual cutting temperature and tool stress will be lower than the simulation predictions. Therefore, the simulation output temperature/stress should be regarded as a conservative upper limit for the parameter window; the fracture experiment of the uncoated tool at 1200/4 confirmed that this upper limit is close to the fracture threshold, while the coated tool can work stably below this upper limit. The AlTi coating thickness is only a few microns, and its influence on the overall thermo-elastic calculation parameters is negligible, so it was not separately distinguished in the simulation model.

2.3. Processing characteristics of gun drill bit

The gun drill bit has a unique geometric structure, exhibiting the following characteristics during the machining process [15]: 1. The drill bit is an incomplete cylinder, with the drill tip not at the geometric center, resulting in uneven wall thickness of the oil passage holes and significant internal stress within the drill bit. 2. The cutting edge portion of the drill bit is subjected to compression and shear, resulting in high torque. 3. The outer cutting edge has a higher cutting speed and thus greater wear, whereas the inner cutting edge has a decreasing cutting speed with its distance from the tool center, resulting in higher compressive stress and an increased likelihood of tool fracture.

3. Drilling Simulation Modeling

3.1. Geometric model and mesh generation

The cutting portion of a gun drill is mainly located at the drill tip; modeling this section can improve computational efficiency while ensuring simulation accuracy [13]. A ∅5 mm gun drill tip model (outer cutting edge/inner cutting edge/eccentricity e = 0.15 mm/oil hole) was taken, and a ∅8 mm×2.5 mm cylindrical workpiece was extracted to represent the quasi-steady-state cutting zone. The drill diameter is 5 mm, and the geometric parameters are shown in Table 3 [16]; the standard cutting angles and three-dimensional structure of the drill tip are illustrated in Fig. 2 and Fig. 3, respectively.

Adaptive mesh refinement was employed for mesh generation [14]. During the drilling process, temperature variations are primarily concentrated at the contact surface between the workpiece and the drill bit; this area is designated as a high-density mesh region (minimum element size in the chip formation zone ≤ 0.1 mm). In contrast, areas

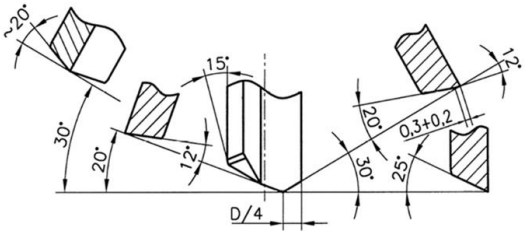

Fig. 2 Standard angles of gun drill

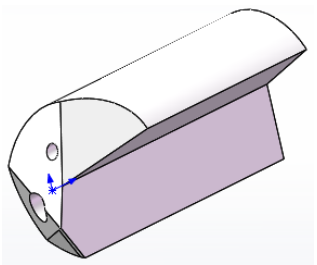

Fig. 3 Three-dimensional structure of drill bit

Table 3
Main geometric parameters of gun drill bit

Parameter	Value	Unit
Drill diameter	5	mm
Eccentricity e	0.15	mm
Outer cutting edge angle	20	°
Inner cutting edge angle	15	°
Oil gap angle	30	°
Back angle of outer blade	10	°

with minimal temperature changes are assigned a low-density mesh. The mesh was dynamically generated through an adaptive refinement strategy to balance computational accuracy and efficiency.

3.2. Constitutive model and material parameters

The drilling depth is set to half the diameter of the gun drill bit, i.e., 2.5 mm [13]. The workpiece is configuredas a cylinder with a diameter of 8 mm and a height of 2.5 mm. The constitutive equation for 15-15hs Max adopts an Arrhenius-type hyperbolic sine form, derived from the flow stress fitting of high-temperature compression tests of high-nitrogen austenitic stainless steel [17]:

$$\dot{\varepsilon} = 3.49\times10^{15}\left[\sinh 0.0059\sigma\right]^{10.94} exp\left(-\frac{524840}{RT}\right). \quad (1)$$

In the formula, ε is the strain rate, s^{-1}; σ is the flow stress, MPa; R is the gas constant, 8.3145 $J\cdot mol^{-1}\cdot K^{-1}$; T is the absolute temperature, K. The unit of the coefficient 0.0059 is MPa^{-1}, ensuring the argument of the *sinh* function is dimensionless.

This constitutive equation describes the high-temperature flow behavior of the material over a wide temperature range and strain rate, and participates in the chip separation calculation in DEFORM through temperature-strain rate mapping. It should be noted that the constitutive parameters were fitted based on compression tests at low strain rates and high temperature ranges; extrapolation to the extremely high strain rates and wide temperature ranges of drilling may introduce some systematic deviations. Given the current lack of a dedicated cutting constitutive model for 15-15hs Max, this Arrhenius form was adopted as an engineering approximation for trend analysis and parameter window definition, with dedicated constitutive parameters to be calibrated through high-speed cutting experiments in future work.

3.3. Boundary conditions and simulation control

The bottom surface of the workpiece is fully constrained; the tool rotates about the Z-axis and feeds along the negative Z-axis; the initial temperature of the workpiece is set to 20 °C. The tool-chip friction model adopts a Coulomb-shear friction mixed mode, with a friction coefficient of 0.75, referring to the conventional range for difficult-to-machine stainless steel drilling simulation [8]. The convective heat transfer coefficient of the exposed workpiece surface to air is set to 15 $W\cdot m^{-2}\cdot K^{-1}$; the convective heat transfer coefficient of the high-pressure cooling fluid flushing region is set to 1000–1500 $W\cdot m^{-2}\cdot K^{-1}$, simulating the actual high-pressure internal cooling conditions (pressure 8.0 MPa, flow rate 10 L/min).

The International System of Units is used, with a total of 10,000 simulation steps and data saved every 25 steps. The simulation terminates upon reaching 10,000 steps or when the drilling depth reaches the preset value. The tool wear model adopts the Usui model [8]:

$$\omega = \int apVe^{-b/T}dt\,. \quad (2)$$

In the formula, ω is the wear volume; T is the absolute temperature; p is the contact pressure; V is the sliding velocity; a and b are test coefficients, set to $a = 1\times10^{-7}$ and $b = 855$ according to empirical values [8]. The simulation model is depicted in Fig. 4.

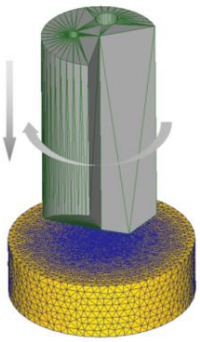

Fig. 4 Grid division and model

4. Analysis of Simulation Results

4.1. Temperature field distribution characteristics

Firstly, the simulation was conducted using the process parameters of 1200 r/min rotational speed and 4 mm/min feed rate, and a graph of drilling temperature versus time was generated through post-processing. Fig. 5 shows the temperature variation of the workpiece. It can be seen that as drilling begins, the temperature of the workpiece starts to rise. When the simulation reaches 10,000 steps, the local maximum temperature at the cutting zone (located at the root of the chip and the tool-chip contact band) reaches approximately 460°C. It should be particularly pointed out that this temperature is the local adiabatic shear hot spot in the chip tearing/separation zone, and does not represent the workpiece base temperature; the quasi-steady-state temperature of the workpiece-tool contact

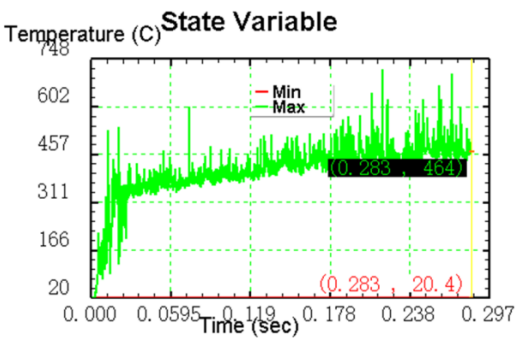

Fig. 5 Workpiece simulation temperature variation diagram

zone/workpiece base under different conditions is 169-213°C (Table 4 and Table 5), which is the temperature indicator of practical engineering significance for tool wear and machining quality.

The temperature variations of the workpiece at the 2500th, 5000th, 7500th, and 10000th steps during the simulation are shown in Fig. 6. As the machining progresses, the workpiece temperature continues to rise, which is caused by the cutting and friction between the tool and the workpiece. The highest temperature of the workpiece is mainly distributed at the bottom of the chip, because the chip is not cooled in time when it is generated, resulting in heat remaining on the chip, and the chip continues to friction with the tool, leading to a higher temperature in this part. Due to the low thermal conductivity of 15-15hs Max (approximately 13.8 $W \cdot m^{-1} \cdot K^{-1}$), the heat diffusion radius is limited, the temperature gradient in the workpiece base is steep, and the heat generated during the machining process is mainly concentrated on the chip and the tool-chip contact zone.

4.2. Single-factor influence of process parameters on temperature

Single-factor simulation experiments were conducted. First, the rotational speed was varied under a given feed rate to obtain the drilling temperatures (quasi-steady-state temperature of the workpiece-tool contact zone) under different rotational speeds, as shown in Table 4. Then, without changing the rotational speed, the drilling temperatures under different feed rates were obtained by varying the feed rate, as shown in Table 5. The single-factor experimental design aims to determine the main effect of each parameter, providing a basis for subsequent process decision-making.

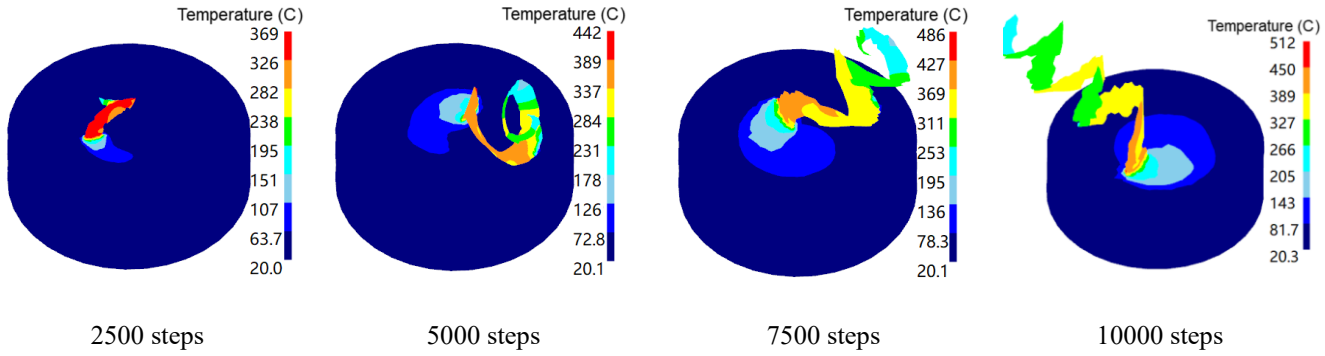

Fig. 6 Schematic diagram of temperature change in drilling area

Table 4

Peak temperature of workpiece (base) under different rotational speeds (feed rate 4 mm/min)

Rotational speed n, $r \cdot min^{-1}$	Peak temperature of workpiece base, °C
600	169.0
800	175.0
1000	183.0
1200	192.5
1400	212.5

Table 5

Peak temperature of workpiece (base) under different feed rates (rotational speed 1200 r/min)

Feed rate f, mm / min	Peak temperature of workpiece base, °C
2	176.0
3	182.0
4	192.5
5	201.0
6	207.4

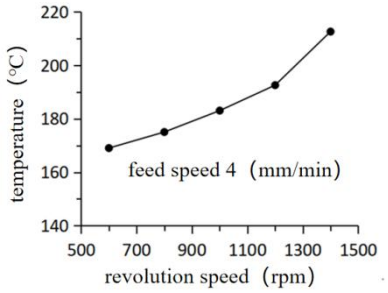

Fig. 7 Effect of rotational speed on temperature

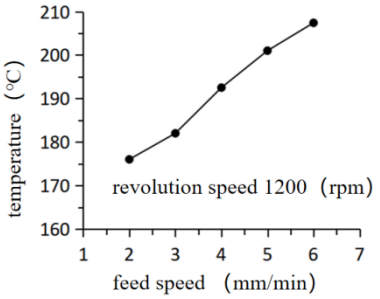

Fig. 8 Influence of feed speed on temperature

As shown in Fig. 7, as the rotational speed increases, the workpiece temperature continues to rise. When the rotational speed increases from 600 r/min to 1400 r/min, $\Delta T \approx +43.5$ °C (+25.7%). This is because as the drilling speed increases, the amount of material removed by the tool from the workpiece per unit time also increases, requiring more energy consumption, which leads to an increase in temperature.

As shown in Fig. 8, as the feed rate increases, the workpiece temperature also rises. When the feed rate increases from 2 mm/min to 6 mm/min, $\Delta T \approx +31.4$ °C (+17.8%). However, compared to the temperature variation caused by an increase in rotational speed, the temperature variation trend caused by an increase in feed rate is relatively smaller. The sensitivity to rotational speed is stronger than to feed, which is consistent with the physical picture of

low-thermal-conductivity materials where "friction frequency/strain rate effects are greater than single-cut depth increment effects".

5. Process Parameter Optimization and Experimental Verification

5.1. Parameter optimization logic and tool breakage boundary analysis

Research indicates that tool rotational speed and feed rate have a significant influence on deep hole tool life [18]; an increase in machining depth also aggravates drill rod vibration, which has an adverse effect on tool life. For special equipment components with extremely high unit value, the primary goal of process optimization is not the highest material removal rate, but ensuring zero tool breakage and hole axis precision. Based on the six groups of data in Table 6, a comprehensive evaluation was conducted from the four dimensions of temperature, axial force, equivalent stress, and efficiency. It should be noted that cases No. 1–4 were preliminary single-factor temperature field studies, and equivalent stress was not calculated; cases No. 5 and 6 were supplemented with thermo-mechanical coupling analysis.

Case 6 (1200 r/min, 5 mm/min) has the highest efficiency (11775 mm³/min), but the workpiece temperature of 201 °C, drill bit equivalent stress of 2819 MPa, and axial force of 80 N are all extreme values among the six groups. Its thermo-mechanical load exceeds the critical threshold (192.5°C, 2601 MPa) at which the uncoated YG8 tool fractured at 1200/4, and the simulation has already classified it as a high-risk zone; no actual cutting verification was performed.

Case 3 (1000 r/min, 5 mm/min) has a higher efficiency (9812 mm³/min) than Case 5, and the temperature of 189.7°C is also relatively low, but the axial force of 81 N is approximately 14% higher than that of Case 5 (71 N). For a slender gun drill with ∅5 mm and $L/D = 240$, a larger axial force will aggravate drill rod vibration, leading to an increased risk of axis deviation. Although a complete stress simulation was not performed for this case, its stability is inferior to Case 5 based on the axial force trend.

Case 5 (1200 r/min, 4 mm/min) has a workpiece temperature of 192.5°C, axial force of 71 N, and equivalent stress of 2601 MPa. This parameter window approaches the tool breakage threshold of the uncoated tool (approximately 670 mm), and the simulation has shown that it is at the thermo-mechanical bearing limit. In actual machining, an AlTi-coated tool was used; since the coating reduces tool-chip friction and heat conduction, the measured thermo-mechanical load is lower than the conservative upper limit predicted by the simulation, and five full-length 1200 mm workpieces were successfully machined with a safety margin.

It is evident that Case 6 is excluded first due to thermo-mechanical overload, Case 3 is excluded due to its relatively high axial force and insufficient stability, and Case 5 achieves the best balance between efficiency and reliability, making it the optimal solution that considers both feasibility and machining efficiency.

Table 6
Comprehensive comparison of candidate parameter schemes

Case	n, r/min	f, mm/min	Peak temperature of workpiece base, °C	Axial force, N	Equivalent stress, MPa
1	600	4	169.0	—	—
2	800	4	175.0	—	—
3	1000	5	189.7	81	—
4	1200	2	176.0	—	—
5	1200	4	192.5	71	2601
6	1200	5	201.0	80	2819

5.2. Full-scale machining experiment

Verification experiments were conducted on a seven-axis deep hole drilling machine, as shown in Fig. 9. The axis deviation of the machined hole was obtained by measuring the wall thickness to verify whether the processed hole met the specifications.



Fig. 9 Experimental gun drilling platform

The drill bit material is cemented carbide, and the cost of a single gun drill is high; the processing object is a special equipment component with extremely high value. Considering the wear of the gun drill bit and the durability of the drill bit, a total of 6 workpieces were machined. The first experiment (uncoated YG8, 1200 r/min, 4 mm/min, tool regrinding every 100 mm) resulted in tool breakage at approximately 670 mm, and this workpiece was scrapped. Subsequently, an AlTi-coated YG8 tool was adopted, with the process parameters maintained at 1200 r/min, 4 mm/min, cutting fluid flow rate 10 L/min, and cutting fluid pressure 8.0 MPa, with tool regrinding every 70 mm. The machined hole dimensions were: diameter 5 mm, length 1200 mm. The AlTi-coated tool completed a total of 5 workpieces×1200 mm full-length machining, with a cumulative cutting length of ≥ 6000 mm per tool edge. Due to the extremely high unit value of the workpieces, this study did not establish a classical Taylor tool life curve (Taylor equation), but instead used the first breakage depth (670 mm) as the tool reliability threshold and zero tool breakage as the process feasibility criterion. Since the coating reduces the actual tool-chip friction and heat conduction into the tool base, the measured thermo-mechanical load is lower than the uncoated limit predicted by the simulation, thus five full-length workpieces were successfully machined. This indicates that although the simulation results cannot directly predict the precise state of the coated tool, they provide a conservative upper limit for the parameter window of the coating process.

Before machining, the tool was ground and clamped, checking whether the cutting edge angle had been

ground to the most suitable processing angle. After grinding, the tool was assembled with a sleeve and bearing, and finally mounted on the tool support rack installed on the machine tool and connected to the spindle. The workpiece was fixed while the tool rotated and fed. The workpiece was secured on the worktable using a support seat, clamping plate, screw rod, nut, and other components, and a lever dial indicator was used to check the straightness of the workpiece clamping. The sleeve hole diameter is slightly smaller than the tool diameter (typically 0.5-1 mm smaller) to ensure positioning accuracy.

After completing the installation of the tool and workpiece, the workpiece and tool were positioned to ensure that the processing axis of the tool coincided with the axis of the workpiece to be machined, avoiding axis deviation that could lead to workpiece scrapping. Fig. 10 shows the tool bit.

As depicted in Fig. 11, the chips expelled during the machining process are short spiral, with smooth surfaces, beneficial for high-pressure oil evacuation, and no chip blockage occurred. Due to the hole diameter of only 5 mm and the length-to-diameter ratio of 240, the internal wall surface roughness was not included in this statistics due to measurement accessibility limitations, and will be supplemented in future work using borescope profilometry or sectioned specimen analysis.



Fig. 10 Tool bit



Fig. 11 Chips discharged during processing

5.3. Hole axis deviation detection and precision verification

After machining, the wall thickness of the workpieces was measured using an ultrasonic thickness gauge to obtain the axis deviation at various depths, as shown in Table 7 (negative values indicate downward inclination, unit mm; measurements were initiated from 300 mm because the workpieces are hollow 240 mm from the front end).

In this experiment (five subsequent workpieces), the maximum axis deviation was 0.70 mm and the minimum was 0.36 mm, with an overall downward inclination. Within the first 600 mm depth, the axis deviation is relatively small, because the gun drill has penetrated a short distance into the workpiece, resulting in better rigidity and less vibration of the drill rod. As the penetration depth increases, the axis deviation gradually increases, mainly because the slender gun drill has poor overall rigidity, and drill rod vibration increases with penetration depth. It is evident that under these parameters, the axis deviation range of the machined deep holes meets the project technical requirement of axis deviation tolerance (±1.0 mm, consistent with general industry precision standards), indicating that the process parameters obtained from the simulation are in accordance with the demands of deep hole drilling.

Table 7

Full-length axis deviation measurement results of five workpieces

No.	300 mm	400 mm	600 mm	800 mm	1000 mm	1200 mm
1	0	0	-0.10	-0.17	-0.31	-0.45
2	0	0	-0.09	-0.31	-0.49	-0.67
3	0	-0.13	-0.21	-0.27	-0.33	-0.58
4	0	-0.04	-0.14	-0.30	-0.42	-0.70
5	0	-0.02	-0.09	-0.14	-0.19	-0.36

6. Conclusions

In this study, gun drilling was used to machine a Ø5 mm×1200 mm deep hole in 15-15hs Max material, and a thermo-mechanical coupling simulation analysis and experimental verification of the drilling process were conducted. The main conclusions are as follows:

1. A thermo-mechanical coupled finite element model of Ø5 mm gun drilling of 15-15hs Max was established, clarifying that cutting heat is concentrated in the tool-chip contact band. The local maximum temperature in the cutting zone (root of chip and tool-chip contact band) reaches approximately 460 °C, which is a local adiabatic shear hot spot; the quasi-steady-state temperature rise of the workpiece base ranges from 169 to 213 °C, which is of practical engineering significance for tool wear and machining quality.

2. Both feed rate and spindle speed are positively correlated with drilling temperature. The influence of rotational speed is more significant: when the rotational speed increases from 600 r/min to 1400 r/min, the workpiece temperature rises from 169 °C to 212.5 °C (increase of 25.7%); when the feed rate increases from 2 mm/min to 6 mm/min, the workpiece temperature rises from 176 °C to 207.4 °C (increase of 17.8%). The ranking of influencing factors from largest to smallest is: spindle speed > feed rate.

3. The first experiment using an uncoated YG8 tool at 1200 r/min, 4 mm/min resulted in tool breakage at approximately 670 mm, indicating that this parameter is close to the thermo-mechanical bearing limit of the uncoated tool. Simulation shows that further increasing the feed to 5 mm/min at 1200 r/min results in higher stress and temperature, with greater risk, so no trial cutting was performed. After replacing with an AlTi-coated tool, since the coating reduces tool-chip friction and heat conduction into the tool base, the actual thermo-mechanical load is lower than the uncoated limit predicted by the simulation, and five full-length workpieces were successfully machined, verifying the engineering guiding value of the simulation parameter window as a "conservative upper limit". The final adoption of 1200 r/min, 4 mm/min with the AlTi-coated tool controlled the workpiece base temperature at 192.5 °C, validating the parameter selection logic that "temperature–stress–reliability constraints take priority over the highest MRR". The 70 mm tool regrinding interval serves as an engineering strategy to ensure tool life, guaranteeing the stability of the machining process.

4. Full-scale machining verification of five workpieces was completed. The machined hole diameter is 5 mm and the length is 1200 mm, with a maximum axis deviation of 0.70 mm, meeting the project technical requirement of axis deviation tolerance (±1.0 mm, consistent with general industry precision standards). The quantitative relationship between rotational speed/feed rate and cutting temperature was established, and the parameter safety window was defined with the tool breakage experiment as the boundary, providing reproducible experimental evidence for the process parameter selection and optimization of gun drilling of 15-15hs Max.

Future work can further explore optimization of cutting edge micro-geometry, upgrading of coating systems, and cooling fluid supply strategies, to maintain tool reliability at higher efficiency, and establish a Taylor-type tool life model through multi-batch statistical verification.

References

1. **Odnobokova, M.V.; Belyakov, A.N.; Dolzhenko, P.D.; Kostina, M.V.; Kaibyshev, R.O.** 2023. On the strengthening mechanisms of high nitrogen austenitic stainless steels, Materials Letters 331: 133502. https://doi.org/10.1016/j.matlet.2022.133502.
2. **He, Z.F.; Sun, L.F.; Guo, Y.X.; Zhao, J.T.; Zhang, H.; Jiang, S.; Yan, H.L.; Zhang, N.; Jia, N.** 2024. Strengthening high-nitrogen austenitic stainless steel via constructing multi-scaled heterostructure, Journal of Materials Research and Technology 32: 2076-2085. https://doi.org/10.1016/j.jmrt.2024.08.059.
3. **Ferreira, V. H. M. M.; Coury, F. G.; de Araujo Santana, D.; Yuuki Koga, G. Y.** 2024. Novel high nitrogen austenitic stainless steels: From high-throughput screening to experimental validation and properties relationship, Journal of Materials Research and Technology 30: 640-656. https://doi.org/10.1016/j.jmrt.2024.03.090.
4. **Gao, F.Y.; Qiao, Y.X.; Chen, J.; Yang, L.L.; Zhou, H.L.; Zheng, Z.B.; Zhang, L.M.** 2023. Effect of nitrogen content on corrosion behavior of high-nitrogen austenitic stainless steel, NPJ Materials Degradation 7(1): 75. https://doi.org/10.1038/s41529-023-00394-x.
5. **Pang, X.H.; Zhang, X.Y.; Liu, Y.L.; Chen, W.** 2011. Experimental Study on Machinability of Nickel-Free High-Nitrogen Austenitic Stainless Steel, Journal of North University of China (Natural Science Edition) 32(5): 561-566. (In Chinese) https://doi.org/10.3969/j.issn.1673-3193.2011.05.007.
6. **Biermann, D.; Bleicher, F.; Heisel, U.; Klocke, F.; Möhring, H. C.; Shih, A. J. M.** 2018. Deep hole drilling, CIRP Annals 67(2): 673-694. https://doi.org/10.1016/j.cirp.2018.05.007.
7. **Yıldız, A.; Kurt, A., Yağmur, S.** 2020. Finite element simulation of drilling operation and theoretical analysis of drill stresses with the Deform-3D, Simulation Modelling Practice and Theory 104: 102153. https://doi.org/10.1016/j.simpat.2020.102153.
8. **Lotfi, M.; Amini, S., Al-Awady, I.Y.** 2018. 3D numerical analysis of drilling process: heat, wear, and built-up edge, Advances in Manufacturing 6(2): 204-214. https://doi.org/10.1007/s40436-018-0223-z.
9. **Zhu, Z.J.; Sun, X.H., Guo, K.; Sun, J.; Li, J.** 2022. Recent advances in drilling tool temperature: a state-of-the-art review, Chinese Journal of Mechanical Engineering 35(1): 148. https://doi.org/10.1186/s10033-022-00818-w.
10. **Feng, S.; Gong, Y.F., Zeng, G.Y.** 2024. Analysis of drilling force and chip in gun drilling of 15-15hs Max material, Tool Engineering 58(5): 67-71. (In Chinese) https://doi.org/10.3969/j.issn.1000-7008.2024.05.012.
11. **Lou, J.C.; Li, L.; Dong, X.F.; Cao, M.Z.; Jiang, J.T.; Zhang, Y.** 2024. Research on the influencing factors of chip forming in 304 stainless steel deep hole gun drilling, The International Journal of Advanced Manufacturing Technology 134(3): 1447-1461. https://doi.org/10.1007/s00170-024-14205-3.
12. **Li, Y.; Wang, Y.; Gao, F.** 2020. Simulation of and experimental study on drilling performance of 304 stainless steel, Journal of Xi'an University of Technology 36(4): 538-543 (In Chinese). https://doi.org/10.19322/j.cnki.issn.1006-4710.2020.04.014.
13. **Klocke, F.; Abouridouane, M.; Gerschwiler, K.; Lung, D.** 2011. 3D Modelling and Simulation of Gun Drilling, Advanced Materials Research 223: 12-19. https://doi.org/10.4028/www.scientific.net/AMR.223.12.
14. **Abouridouane, M.; Klocke, F.; Oktafiani A.; Döbbeler, B.** 2017. Microstructure-based FEM Simulation of Metal Cutting, Procedia CIRP 58: 85-90. https://doi.org/10.1016/j.procir.2017.03.336.
15. **Zhang, Y.; Li, L.; Xie, C.; Lou, J.C.** 2022. The theoretical model of straightness error in gun drilling of small diameter and deep hole, The International Journal of Advanced Manufacturing Technology 122(7): 3447-3465. https://doi.org/10.1007/s00170-022-10089-3.
16. **Hussain, A.; Sharif, A.; Siddiqi, M.U.R.; Hussain, G.; Getachew, M.T.; Muhammad, R.** 2024. Deform 3D Simulation and Experimental Study in Machining of AISI 1020 Mild Steel, Journal of Engineering 2024: 9085919. https://doi.org/10.1155/2024/9085919.
17. **Ji, S.** 2017. Basic research on hot deformation behavior technology of high nitrogen nickel-free austenitic stainless steel. North China University of Science and Technology.
18. **Pollák, M.; Kočiško, M.; Petrus, J.; Grozav, S.D.; Ceclan, V.** 2022. Research into the Impact of Spindle Speed and Feed Rate Changes on the Life of a Deep-Drilling Technology Tool, Machines 10(4): 268. https://doi.org/10.3390/machines10040268.
19. American Petroleum Institute. 2023. Specification for Rotary Drill Stem Elements, API Specification 7-1. 2nd ed. Washington, DC: American Petroleum Institute.

S. Feng, Y. Gong, G. Zeng

THERMO-MECHANICAL COUPLING SIMULATION AND PROCESS RESEARCH OF GUN DRILLING FOR 15-15HS MAX HIGH-NITROGEN NON-MAGNETIC STEEL WITH ULTRA-LARGE LENGTH-TO-DIAMETER RATIO

S u m m a r y

High-nitrogen austenitic stainless steel 15-15hs Max (UNS S20910) exhibits excellent resistance to sulfide stress corrosion cracking and a high yield strength (≥1118 MPa), and is widely used in key components of energy equipment, aerospace, and chemical industries. However, its room-temperature thermal conductivity is only about 13.8 $W \cdot m^{-1} \cdot K^{-1}$ and significant work hardening occurs, which readily induces cutting heat accumulation and tool failure during gun drilling of deep holes with a diameter of Ø5 mm and a length-to-diameter ratio of 240∶1. In this study, a local thermo-mechanical coupled finite element model of the Ø5 mm gun drill tip was established using DEFORM-3D, and the influence of rotational speeds from 600 to 1400 r/min and feed rates from 2 to 6 mm/min on the cutting zone temperature field and tool equivalent stress was systematically analyzed. The simulation results show that the instantaneous local hot spot at the root of the chip in the cutting zone can reach approximately 460°C, while the quasi-steady-state temperature rise of the workpiece base ranges from 169 to 213°C; the influence of rotational speed on the temperature rise is significantly greater than that of the feed rate. In the first trial cut, an uncoated YG8 tool fractured at approximately 670 mm. After replacing with an AlTi-coated tool, full-scale trial cutting verified the reliability of the parameter window; five workpieces of full length 1200 mm were successfully machined without tool breakage, and the hole axis deviation ranged from 0.36 to 0.70 mm, meeting the project technical requirement of axis deviation tolerance (±1.0 mm, consistent with general industry precision standards). The quantitative relationship between rotational speed/feed rate and cutting temperature was established, and the parameter safety window was defined with temperature–stress–tool breakage as constraint boundaries, providing reproducible experimental evidence for the process parameter selection of gun drilling of 15-15hs Max.

Keywords: deep hole gun drilling, 15-15hs Max, high-nitrogen non-magnetic steel, thermo-mechanical coupling, cutting temperature, tool reliability.

Received December 2, 2024
Accepted October 15, 2026

This article is an Open Access article distributed under the terms and conditions of the Creative Commons Attribution 4.0 (CC BY 4.0) License (http://creativecommons.org/licenses/by/4.0/).